Acta Cryst. (1981). A**37**, 769–774

Silicon-Crystal Rocking Curves under X-ray Acoustic Resonance Conditions

BY I. R. ENTIN AND K. P. ASSUR

Institute of Solid State Physics, Academy of Sciences of the USSR, 142432 Chernogolovka, Moscow district, USSR

(*Received* 18 *September* 1980; *accepted* 7 *April* 1981)

Abstract

Silicon-crystal rocking curves are measured with a high angular resolution (~0·1″) under conditions of the Borrmann effect resonant suppression by transverse ultrasonic vibrations. It is shown that on the curves deep minima appear whose positions depend on the vibrational frequency, in agreement with the theory.

Introduction

The effect of ultrasonic vibrations on X-ray diffraction in perfect crystals was observed both in the case of long ultrasonic waves, $K_S \ll |\Delta K^0|$ ($\mathbf{K}_S$ is the wave vector of the ultrasound, $\Delta\mathbf{K}^0$ is the minimum value of the splitting $\Delta\mathbf{K}$ of the dynamical diffraction dispersion surface), and for short ultrasonic waves, $K_S \gg |\Delta K^0|$. For small absorption local intensity changes of the diffraction spot and the reflection integral intensity increase were found in the first region (Haruta, 1967) and in the second region satellites whose positions were in agreement with the kinematic diffraction theory were observed on the rocking curves (Köhler, Möhling & Peibst, 1974; LeRoux, Colella & Bray, 1975). In thick crystals ultrasonic vibrations suppress X-ray anomalous transmission (Saccocio, Lopez & Lazara, 1967; Hauer & Burns, 1975; LeRoux, Colella & Bray, 1976). The dependence of these diffraction effects on $\mathbf{K}_S$ was not of resonance nature.

Resonance was found and studied in the intermediate region of ultrasonic wavelengths (Entin, 1977, 1978*a*,*b*; Entin, Suvorov, Kobelev & Soifer, 1978). It was shown that a transverse ultrasonic wave with a wave vector lying in the reflecting plane causes the Borrmann effect resonant suppression when satisfying the condition

$$\mathbf{K}_S = \mathrm{Re}(\Delta\mathbf{K}). \qquad (1)$$

The divergence of X-ray radiation incident on the crystal (2–3′) exceeded by two orders the angular width of the reflection maximum (~1″) in that case. All points on the dispersion sheet near the Brillouin zone boundary were excited and the trajectories of the Bloch waves in the crystal lay within the Borrmann triangle in the angular range $2\theta_B$ (θ_B is the Bragg angle). Experimental results consisted, firstly, of a sharp reduction of integral (over the Borrmann triangle base) intensity of the diffracted beam, when the ultrasound wavelength λ_S was equal to the extinction length τ ($\tau = |\Delta K^0|^{-1}$) and, secondly, of the appearance of the decreased intensity bands on the topograms, their positions radically depending on the acoustic vibration frequency. These effects took place under a very weak acoustic influence (the displacement amplitude was ~10^{-3} Å, the deformation amplitude was 10^{-9}–10^{-8}).

Resonance is determined by interzone scattering, mixing the Bloch states on the upper and lower branches of the dispersion surface and increasing the effective absorption coefficient of the weakly absorbed field. Condition (1) expresses the quasimomentum conservation law and selects the tie points for which the anomalous transmission is suppressed (Fig. 1). If

$$\mathbf{K}_S = \mathrm{Re}(\Delta\mathbf{K}^0) \quad (\lambda_S = \tau),$$

the ray propagating along the reflecting plane and making the greatest contribution to the integral intensity of the reflection at a thick crystal is extinguished. The integral intensity decrease is maximum

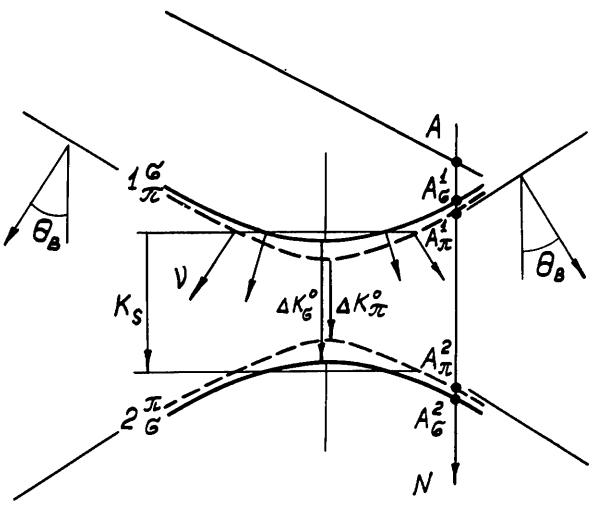

Fig. 1. Dispersion surface in the two-beam case. *A* entrance point; **v** group velocity vector.

0567-7394/81/060769-06$01.00

here and the decreased intensity band is in the center of the topogram. When

$$\mathbf{K}_S = \mathrm{Re}(\Delta\mathbf{K}) > \mathrm{Re}(\Delta\mathbf{K}^0) \quad (\lambda_S < \tau),$$

the central band splits into two side bands whose positions are determined by the group velocity directions at the corresponding tie points. Since the X-ray beam incident on the crystal is not polarized and the dispersion surfaces for σ- and π-polarization radiation do not coincide, doubling of the number of intensity minima is observed. The use of this effect for a direct study of the shape of the dynamical diffraction dispersion surface has been proposed (Entin, 1978*a*).

These experimental results suggest that provided a practically parallel X-ray beam is incident on the crystal (the divergence being substantially smaller than the angular width of the dynamical diffraction maximum) the resonance condition (1) should be satisfied for definite values of the angular deviation $\Delta\theta$ from the center of the diffraction maximum, so that the shape of the diffracted- and transmitted-beam rocking curves should change essentially compared to an undistorted crystal. In this connection the purpose of the present paper is to study the rocking-curve shape with high angular resolution under X-ray acoustic resonance conditions.

Theory

The X-ray acoustic resonance theory was developed (Entin, 1978*b*) on the basis of the Takagi (1962) equation system analysis for the case of a sinusoidal displacement field. Another approach to the problem involves the multiwave dynamical diffraction theory (Entin, 1979). Here we review briefly the results of the latter approach (the case $K_S \gg |\Delta K^0|$ was considered by Köhler, Möhling & Peibst, 1974).

The crystal reciprocal lattice with a standing displacement wave

$$\mathbf{u} = \mathbf{v}\sin(2\pi\mathbf{K}_S\,\mathbf{r}),$$

where

$$\mathbf{v} = \mathbf{v}_0\sin(2\pi f T),$$

f is the ultrasonic frequency, contains, in addition to the principal points $\mathbf{H}$, satellites $\mathbf{H} \pm n\mathbf{K}_S$, the corresponding polarizability Fourier component being

$$\chi_{\mathbf{H}+n\mathbf{K}_S} = (-1)^n J_n\{2\pi(\mathbf{H} + n\mathbf{K}_S)\,\mathbf{v}\}\,\chi_{\mathbf{H}}^P,$$

where $J_n(x)$ is the nth-order Bessel function, $\chi_{\mathbf{H}}^P$ is the Fourier component of the undistorted crystal polarizability. When $(\mathbf{H}\mathbf{v}_0) \ll 1$ the coefficients $\chi_{\mathbf{H}\pm n\mathbf{K}_S}$ with $n > 1$ can be neglected. In addition, $K_S \ll H$, the coefficients $\chi_{\pm\mathbf{K}_S}$ are also negligibly small (for a transverse acoustic wave they are exactly equal to zero).

If the crystal is in the reflecting position then simultaneously with the points O and $\mathbf{H}$ the points $\pm\mathbf{K}_S$ and $\mathbf{H} \pm \mathbf{K}_S$ are close to the Ewald sphere, and the diffraction becomes multiwave. The form of the dispersion surface (Fig. 2) follows directly from the fact that the length of the reciprocal-lattice cell of the crystal with periodic displacement field in the $\mathbf{K}_S$ direction is equal to K_S and the dispersion surface is periodic in reciprocal space with this period. The largest changes of eigenvalues occur when the dispersion branches intersect, the perturbation lifting (partially or fully) the degeneracy due to the self-intersection. The substantial changes of the eigenvalues at small $\mathbf{v}_0$ determine resonance effects. The imaginary part of the correction to the eigenvalues, resonantly depending on the K_S value, causes the suppression of the anomalous transmission of X-rays. The intensity decrease is described by the factor $[\mathbf{H}\mathbf{v}_0 \ll \mathrm{Im}(\chi_{\mathbf{H}})/\mathrm{Re}(\chi_{\mathbf{H}})]$

$$\frac{\langle J_{0(\mathbf{H})}(\mathbf{v})\rangle_T}{J_{0(\mathbf{H})}(0)} = \exp(-rt)\,I_0(rt), \tag{2}$$

where $J_{0(\mathbf{H})}(\mathbf{v})$ is the instantaneous intensity value of the transmitted (diffracted) beam, $\langle\ldots\rangle_T$ is the average over the vibration period, $I_0(x)$ is the Bessel function of a zero-order imaginary argument,

$$r = \frac{\pi^3|\mathbf{H}\mathbf{v}_0|^2[\mathrm{Re}(\Delta K^0)]^2\,\mathrm{Im}(\Delta K)}{2\{[\mathrm{Re}(\Delta K) - K_S]^2 + [\mathrm{Im}(\Delta K)]^2\}}, \tag{3}$$

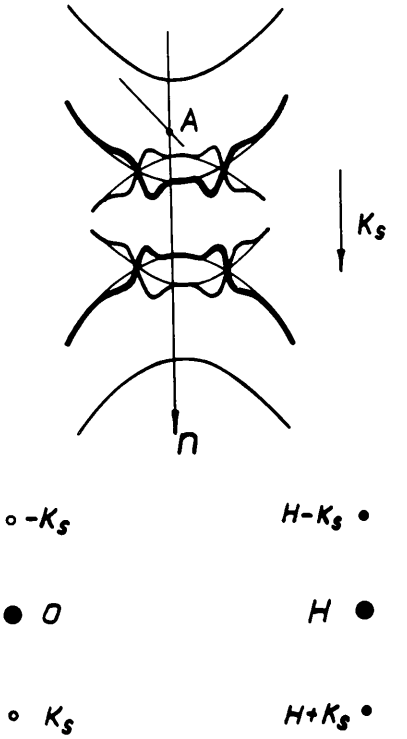

Fig. 2. Dynamical dispersion surface for a crystal with a periodic displacement field (for one of the polarization states).

t is the crystal thickness. Resonance condition (1) follows from (3).

The real part of the correction to the eigenvalues causes dispersion-type effects (Fig. 2). When

$$\frac{C}{2\lambda \cos\theta_B} |\chi_{H+K_S}| > \tfrac{1}{2} \operatorname{Im}(\Delta K_{\sigma(\pi)}),$$

where the subscript σ or π indicates the polarization state, $C = 1$ or $|\cos 2\theta_B|$ for σ or π polarization, λ is the X-ray wavelength, the degeneracy of the real parts of the eigenvalues is lifted and branches do not intersect.

It should be noted that the intersections of the dispersion branches correspond to the centers of the satellites, appearing in the presence of the superlattice. Their angular positions, as can be seen, differ from the positions calculated in the kinematic approximation (the limitation of the kinematic approach to the problem of the satellite positions was remarked by Hapachev, Kolpakov, Kuznetsov & Kuzmin, 1979). In the examined region of the ultrasound wavelengths $\lambda_S \sim \tau$ the satellites are within the structural maximum angular width. So the main effect observed in the case of large μt (μ is the linear absorption coefficient) is anomalous transmission resonant suppression.

Resonance condition (1) can be presented in a form which is more suitable for our purposes, provided $\operatorname{Re}(\Delta K)$ is expressed in terms of the deviation parameter η:

$$\operatorname{Re}(\Delta K_{\sigma(\pi)}) = \frac{C \operatorname{Re}(\chi_H)}{\lambda \cos\theta_B} (1 + \eta^2)^{1/2},$$

where

$$\eta = \Delta\theta \frac{\tau_{\sigma(\pi)}}{d}.$$

d is the interplanar spacing. Hence, for the resonant value of angular deviation, we obtain

$$\Delta\theta^*_{\sigma(\pi)} = \frac{d}{\tau_{\sigma(\pi)}} \left\{ \left(\frac{f\tau_{\sigma(\pi)}}{C_S} \right)^2 - 1 \right\}^{1/2}, \qquad (4)$$

C_S is the sound velocity.

The resonance interpretation in terms of interzone scattering, equivalent to the above-stated one, is that when satisfying condition (1) the strongly absorbed waves excited on the adjacent oscillations of the displacement field interfere constructively (the phase difference is equal to 2π). Effective interference occurs on the absorption length L of the strongly absorbed field, $L \simeq (2\mu)^{-1}$. Such an approach allows one to answer the question whether the limitation of the width S of the incident-wave coherent front leads to resonance smearing. Smearing does not occur if the trajectories of the secondary waves excited on different parts of the path L do not diverge at a distance exceeding S. Hence,

$$2L \tan\alpha < S,$$

where α is the angle between a trajectory and the reflecting plane. With Si (220) reflection, Ag $K\alpha$ radiation and $S = 100$ μm this condition is satisfied if $\eta < 0{\cdot}5$.

Experimental procedure

The experimental arrangement is shown in Fig. 3. Silver radiation is incident on the first Si crystal through 100 and 50 μm wide slits 1, 2 at the Bragg angle for 220 reflection. For obtaining a high angular resolution the double-crystal technique devised by Authier (1961) was applied: slit 3 selected the central ray of the fan formed in the first crystal. This ray was incident on the second crystal. A beam transmitted as well as diffracted by the first crystal could be used here. In the second crystal used as a specimen a transverse

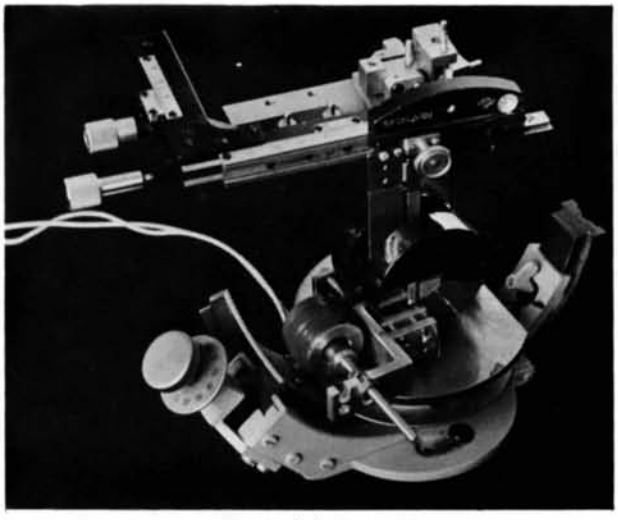

(*a*)

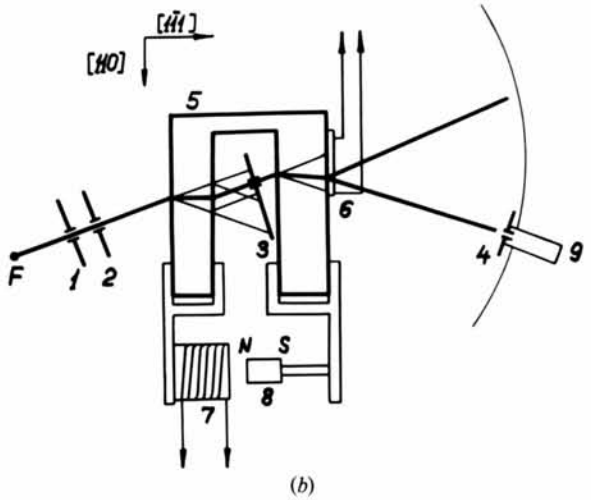

(*b*)

Fig. 3. Photograph of the device (*a*) and its schematic representation (*b*).

ultrasonic wave with a wave vector perpendicular to the entrance surface and a polarization vector directed along the diffraction vector could be excited by means of a quartz transducer (6). The transducer absorbed no more than 10% of the incident radiation.

Preliminary experiments showed that a conventional double-crystal diffractometer with independent axes did not provide mechanical and temperature stability of the crystal setting necessary for our purposes. Therefore, by analogy with Hart & Milne's (1971) technique, both diffracting elements are parts of the same monolithic block (5) of dislocation-free silicon, the thickness of the wafers being 10·8 and 10·7 mm. The distance between the wafers is approximately 10 mm.

The relative orientation of the wafers is changed with the aid of a magnetic coil (7) and a permanent magnet (8). The bending of a thinner (6 mm) crosspiece between the wafers is proportional to the current in the coil.

The width S of slit 3 is chosen because of the following consideration. The beam divergence is determined by the angle 2α of the fan of rays selected by the slit on the one hand and by the diffraction by the slit on the other. Neglecting diffraction we get for angular divergence, with the general formulae of the dynamical diffraction theory (Batterman & Cole, 1964),

$$\Delta\theta' = 2p(1-p^2)^{-1/2}\, d/\tau,$$

where

$$p = \tan\alpha/\tan\theta_B,$$

$$\alpha \simeq \frac{S}{2t_1 \cos\theta_B},$$

t_i is the thickness of the ith wafer.

Hence, with $\alpha \ll \theta_B$, we get

$$\Delta\theta' \simeq Sd/t_1\,\tau \sin\theta_B.$$

The diffraction divergence estimate is given by

$$\Delta\theta'' \simeq \lambda/S.$$

Apparently divergence is minimal when $\Delta\theta' \simeq \Delta\theta''$, and we obtain for the slit optimal width

$$S_{\text{optimal}} \simeq (\lambda t_1 \tau \sin\theta_B/d)^{1/2}.$$

For Si (220) reflection with Ag $K\alpha_1$ radiation and $t_1 =$ 10·8 mm we have $S_{\text{optimal}} \simeq 100$ μm and $\Delta\theta \simeq 0{\cdot}1''$. In our experiments the slit width approximated 150 μm.

To calibrate the angular disorientation $\Delta\theta$ of the wafers in terms of the current i in the coil, the ray displacement Δx at the second-wafer exit surface was measured as a function of the current (since $\mu t \simeq 7{\cdot}5$ only a weakly absorbed ray corresponding to a definite tie point on the upper dispersion hyperbola reached the exit surface). When obtaining the curves in Fig. 4 a counter with a 100 μm wide slit (4) operated in a step-scanning mode within the narrow angular range around $2\theta_B$ (or zero). From the value Δx the angle α between the ray and the reflecting plane

$$\tan\alpha = \Delta x/t_2$$

and the angular deviation values

$$\Delta\theta = p(1-p^2)^{-1/2}\, d/\tau$$

were derived. Since our experimental resolution proved insufficient for observing separation of σ- and π-polarization trajectories, the average extinction length was substituted in the latter formula. It follows from the results represented in Fig. 5 that

$$\Delta\theta\,('') \simeq (0{\cdot}85 \pm 0{\cdot}05)\, i\ (\text{Å}).$$

The rocking curves were obtained with a 'wide open' detector. For recording of the transmitted-beam rocking curves, the detector was set at an angle approxi-

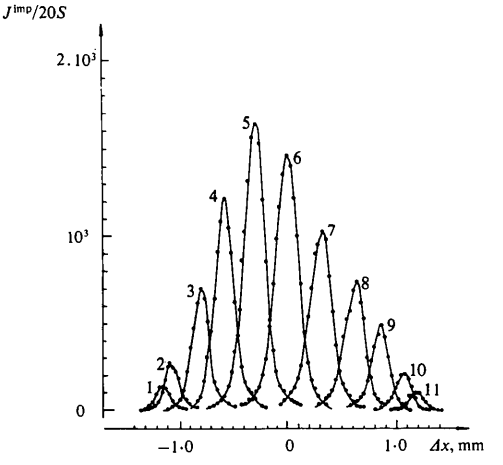

Fig. 4. Beam displacement as a function of the current in the magnetic coil: (1) $i = -1$ A; (2) $i = -0{\cdot}8$ A; (3) $i = -0{\cdot}6$ A; (4) $i = -0{\cdot}4$ A; (5) $i = -0{\cdot}2$ A; (6) $i = 0$; (7) $i = 0{\cdot}2$ A; (8) $i = 0{\cdot}4$ A; (9) $i = 0{\cdot}6$ A; (10) $i = 0{\cdot}8$ A; (11) $i = 1$ A.

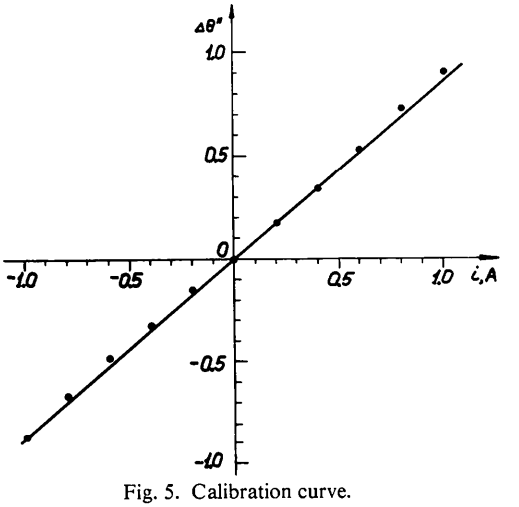

Fig. 5. Calibration curve.

mating zero, if slit 3 selected the beam transmitted by the first wafer, or at an angle approximating $2\theta_B$, if the diffracted beam was used. Recording of the diffracted-beam rocking curves was carried out with the detector set at $2\theta_B$ in the first case and at zero angle in the second case.

Experimental results and discussion

Fig. 6 shows the main experimental results. Curves 1(*a*) and 1(*b*) obtained with the oscillators switched off are compared with the theoretical curves (Fig. 7, 1*a* and 1*b*) given by the general formulae of the dynamical diffraction theory (Batterman & Cole, 1964):

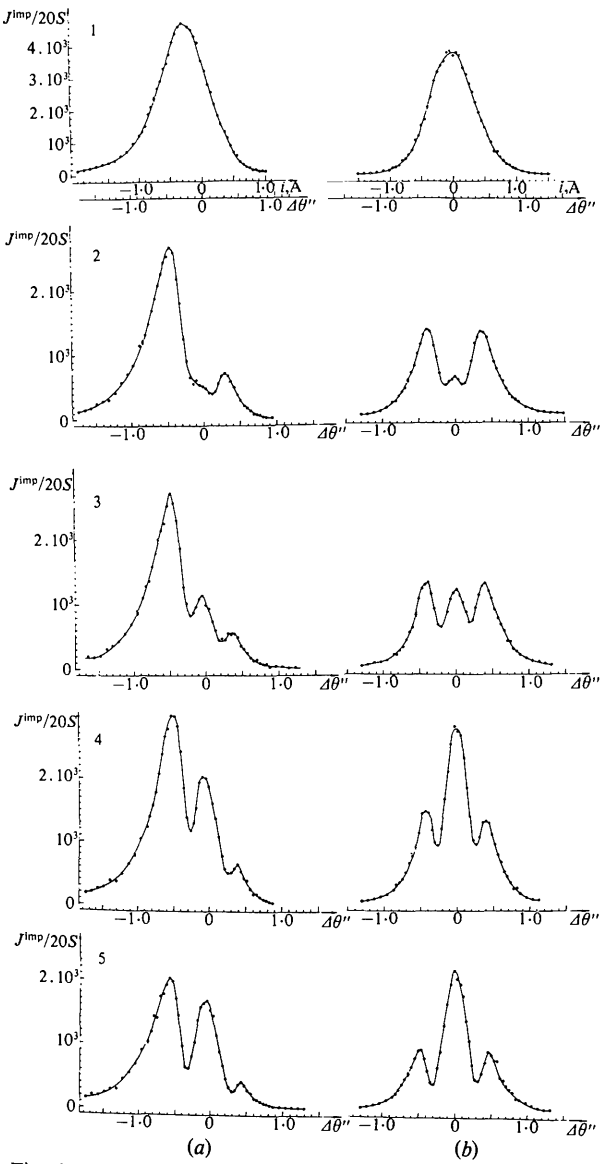

Fig. 6. Transmitted- (*a*) and diffracted- (*b*) beam rocking curves. (1) Generator is switched off; (2) $f = 108{\cdot}97$ MHz; (3) $f = 111$ MHz; (4) $f = 113{\cdot}08$ MHz; (5) $f = 115{\cdot}08$ MHz.

$$J_0 = \tfrac{1}{4}\sum_{\sigma,\pi} J_{\sigma(\pi)}[1-\eta(1+\eta^2)^{-1/2}]^2 \exp\left\{-\frac{\mu t_2}{\cos\theta_B} \times [1-C\varepsilon(1+\eta^2)^{-1/2}]\right\},$$

$$J_{\mathrm{H}} = \tfrac{1}{4}\sum_{\sigma,\pi} J_{\sigma(\pi)}(1+\eta^2)^{-1} \exp\left\{-\frac{\mu t_2}{\cos\theta_B} \times [1-C\varepsilon(1+\eta^2)^{-1/2}]\right\}, \quad (5)$$

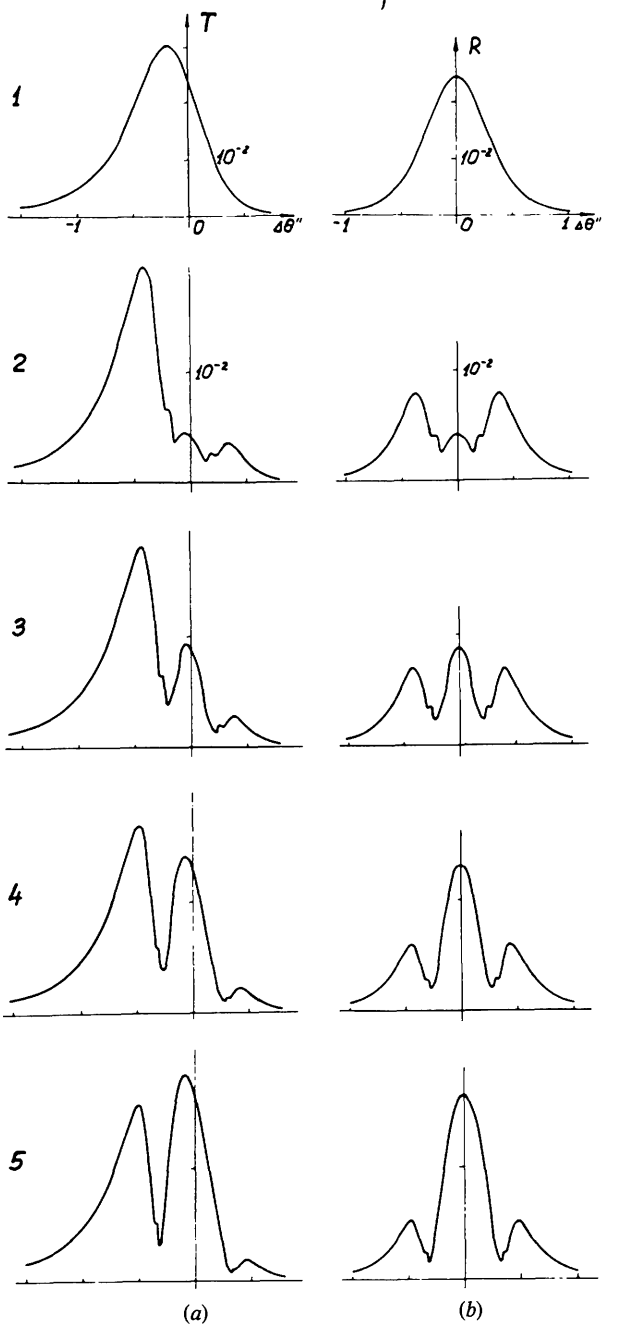

Fig. 7. Theoretical rocking curves for the same cases as in Fig. 6, $|\mathbf{H}\nu_0| = 0{\cdot}01$.

where J_0, J_H and $J_{\sigma(\pi)}$ are the intensities of the transmitted, diffracted and the second wafer incident beams,

$$J_{\sigma(\pi)} = \frac{J}{8} \exp\left[-\frac{\mu t_1}{\cos \theta_B} (1 - C\varepsilon) \right],$$

J is the primary beam intensity,

$$\varepsilon = \mathrm{Im}(\chi_H)/\mathrm{Im}(\chi_0).$$

For Si (220) reflection with Ag $K\alpha$ radiation, $\varepsilon \simeq 0{\cdot}96$ (Batterman & Cole, 1964).

The transmitted beam intensity peaks at $\Delta\theta = -0{\cdot}24 \pm 0{\cdot}02''$ compared to a calculated value of $\Delta\theta = -0{\cdot}18''$. The half-width is equal to $0{\cdot}82 \pm 0{\cdot}06''$, whereas the theoretical value is $0{\cdot}72''$. The measured and theoretical values of the half-width of the diffracted-beam rocking curve are $0{\cdot}74 \pm 0{\cdot}05''$ and $0{\cdot}66''$, respectively. The given error values are mainly determined by the inaccuracy of the angular deviation calibration.

With the excitation of ultrasonic vibrations in the second wafer deep minima occur on the curves. Their positions are sensitive to the ultrasonic frequency: the angular distance between the minima increases with the frequency.

The appearance of the minima on the curves can be explained in the following manner. With incidence angle variation a tie point moves along the dispersion hyperbola, conforming to an anomalously weak absorption. For a definite value $\Delta\theta$, depending on the ultrasonic wavelength, the resonance condition (4) is satisfied, and the effective absorption coefficient increases. Since the incident radiation is not polarized, in a general case there should be four minima on the rocking curves. The separation of minima due to polarization is small, however, and is not observed in our case.

The corresponding theoretical curves (Fig. 7, curves 2*a*,*b*–5*a*,*b*) are obtained by multiplying the right of equations (5) by the factor (2). It is assumed that $\tau_\sigma = 46{\cdot}8$ and $\tau_\pi = 48{\cdot}9$ μm (Tanemura & Kato, 1972), and the velocity of transverse elastic waves in silicon in the [111] direciton is $C_S = 5{\cdot}09 \times 10^3$ m s^{-1} (McSkimin & Andreatch, 1964). As seen from Table 1 the observed and calculated values of the angular distance between the minima are in good agreement.

The obtained results show that rocking-curve measurement represents a technique of X-ray acoustic resonance observation. This technique as well as integral intensity measurement and topography (Entin, 1978*b*) permit the measurement of the parameters of X-ray dynamical diffraction and the study of the dispersion surface shape. In addition, the results allow a possibility of effectively controlling an X-ray beam by means of a weak acoustic influence.

Table 1. *Observed and calculated values of the angles ('') between the intensity minima on the rocking curves*

f(MHz)	Observed	Calculated
108·97	0·22 ± 0·02	0·26
111·00	0·42 ± 0·03	0·43
113·08	0·54 ± 0·03	0·54
115·08	0·63 ± 0·04	0·64

References

AUTHIER, A. (1961). *Bull. Soc. Fr. Minéral. Cristallogr.* **84**, 51–103.

BATTERMAN, B. W. & COLE, H. (1964). *Rev. Mod. Phys.* **36**, 681–717.

ENTIN, I. R. (1977). *Pis'ma Zh. Eksp. Teor. Fiz.* **26**, 392–395; *JETP Lett.* **26**, 269–272.

ENTIN, I. R. (1978*a*). *Fiz. Tverd. Tela*, **20**, 2130–2133; *Sov. Phys. Solid State*, **20**, 1230–1232.

ENTIN, I. R. (1978*b*). *Phys. Status Solidi B*, **90**, 575–584.

ENTIN, I. R. (1979). *Zh. Eksp. Teor. Fiz.* **77**, 214–222; *Sov. Phys. JETP*, **50**, 110–114.

ENTIN, I. R., SUVOROV, E. V., KOBELEV, N. P. & SOIFER, YA. M. (1978). *Fiz. Tverd. Tela*, **20**, 1311–1315; *Sov. Phys. Solid State*, **20**, 754–756.

HAPACHEV, YU. P., KOLPAKOV, A. V., KUZNETSOV, G. F. & KUZMIN, R. N. (1979). *Kristallografiya*, **24**, 430–438.

HART, M. & MILNE, A. D. (1971). *Acta Cryst.* A**27**, 430–435.

HARUTA, K. (1967). *J. Appl. Phys.* **38**, 3312–3316.

HAUER, A. & BURNS, S. J. (1975). *Appl. Phys. Lett.* **27**, 524–526.

KÖHLER, R., MÖHLING, W. & PEIBST, H. (1974). *Phys. Status Solidi B*, **61**, 173–180.

LEROUX, S. D., COLELLA, R. & BRAY, R. (1975). *Phys. Rev. Lett.* **35**, 230–234.

LEROUX, S. D., COLELLA, R. & BRAY, R. (1976). *Phys. Rev. Lett.* **37**, 1056–1059.

MCSKIMIN, H. J. & ANDREATCH, P. (1964). *J. Appl. Phys.* **35**, 2161–2165.

SACCOCIO, E. J., LOPEZ, M. A. & LAZARA, K. J. (1967). *J. Appl. Phys.* **38**, 309–312.

TAKAGI, S. (1962). *Acta Cryst.* **15**, 1311–1312.

TANEMURA, S. & KATO, N. (1972). *Acta Cryst.* A**26**, 69–80.